Petroleum Science 21 (2024) 1875–1888

Contents lists available at ScienceDirect

Petroleum Science

journal homepage: www.keaipublishing.com/en/journals/petroleum-science

Original Paper

Supramolecular polymer-based gel fracturing fluid with a double network applied in ultra-deep hydraulic fracturing

Yong-Ping Huang [a, b], Yong Hu [c], Chang-Long Liu [d], Yi-Ning Wu [a, *], Chen-Wei Zou [a, b], Li-Yuan Zhang [b, **], Ming-Wei Zhao [b], Cai-Li Dai [a, b, ***]

[a] School of Petroleum Engineering, China University of Petroleum (East China), Qingdao, 266580, Shandong, PR China
[b] Shandong Key Laboratory of Oilfield Chemistry, China University of Petroleum (East China), Qingdao, 266580, Shandong, PR China
[c] SINOPEC Petroleum Exploration and Production Research Institute, Beijing, 102206, PR China
[d] CNOOC China Co Ltd, Tianjin Branch, Tianjin, 300459, PR China

ARTICLE INFO

Article history:
Received 15 November 2023
Received in revised form
20 March 2024
Accepted 21 March 2024
Available online 22 March 2024

Edited by Yan-Hua Sun

Keywords:
Ultra-deep reservoir
Gel fracturing fluid
Double network
Supramolecular polymer system
Proppant suspension property

ABSTRACT

A gel based on polyacrylamide, exhibiting delayed crosslinking characteristics, emerges as the preferred solution for mitigating degradation under conditions of high temperature and extended shear in ultra-long wellbores. High viscosity/viscoelasticity of the fracturing fluid was required to maintain excellent proppant suspension properties before gelling. Taking into account both the cost and the potential damage to reservoirs, polymers with lower concentrations and molecular weights are generally preferred. In this work, the supramolecular action was integrated into the polymer, resulting in significant increases in the viscosity and viscoelasticity of the synthesized supramolecular polymer system. The double network gel, which is formed by the combination of the supramolecular polymer system and a small quantity of Zr-crosslinker, effectively resists temperature while minimizing permeability damage to the reservoir. The results indicate that the supramolecular polymer system with a molecular weight of (268–380) $\times$ 10^4 g/mol can achieve the same viscosity and viscoelasticity at 0.4 wt% due to the supramolecular interaction between polymers, compared to the 0.6 wt% traditional polymer (hydrolyzed polyacrylamide, molecular weight of 1078 $\times$ 10^4 g/mol). The supramolecular polymer system possessed excellent proppant suspension properties with a 0.55 cm/min sedimentation rate at 0.4 wt%, whereas the 0.6 wt% traditional polymer had a rate of 0.57 cm/min. In comparison to the traditional gel with a Zr-crosslinker concentration of 0.6 wt% and an elastic modulus of 7.77 Pa, the double network gel with a higher elastic modulus (9.00 Pa) could be formed only at 0.1 wt% Zr-crosslinker, which greatly reduced the amount of residue of the fluid after gel-breaking. The viscosity of the double network gel was 66 mPa s after 2 h shearing, whereas the traditional gel only reached 27 mPa s.

1. Introduction

Deep reservoirs account for the majority of new oil and gas reserves globally, representing a significant source of growth for oil and gas production (Luo et al., 2023; Wang et al., 2022; Xu et al., 2022). The overlying pressure at such depths results in a typically low permeability, particularly in ultra-deep reservoirs (> 6000 m). For example, the permeability of the Fuman (7400–8200 m) and Yuanbei (6500–7100 m) oil and gas fields is 0.1–2 and 0.62 mD, respectively. This limited permeability presents challenges for the flow of oil and gas, often making the expected recovery unattainable (Wu et al., 2023). Hydraulic fracturing is an important method to develop ultra-deep reservoirs efficiently (Gao et al., 2023; Wang et al., 2023; Yang et al., 2022). Fracturing fluids are pivotal in fracturing, transferring pressure, and carrying proppant (Xu et al., 2023). However, high temperature, shear degradation, high friction, and reservoir damage are the challenges of fracturing fluids in ultra-deep reservoirs (Shu and Yan, 2008; Somoza et al., 2023).

Maintaining the structural integrity of fracturing fluids at high

* Corresponding author.
** Corresponding author.
*** Corresponding author. School of Petroleum Engineering, China University of Petroleum (East China), Qingdao, 266580, Shandong, PR China.
E-mail addresses: wuyining@126.com (Y.-N. Wu), 20210085@upc.edu.cn (L.-Y. Zhang), daicl@upc.edu.cn (C.-L. Dai).

https://doi.org/10.1016/j.petsci.2024.03.018

temperatures is the initial step toward addressing the challenges (Alarawi et al., 2023; Hu et al., 2019). Crosslinked polysaccharide gels are usually prescribed to transport proppant from the surface to the target reservoir zones. Among these gels, guar and its derivatives are the most widely used due to their exceptional performance (Biheri and Imqam, 2022; Zhang H. et al., 2018). Guar-based gel fracturing fluids have been successfully utilized in numerous wells for many years (Huang et al., 2019). Nonetheless, the upper-temperature limit of guar-based gels stands at 180 °C, beyond which the glucoside bond within guar becomes highly unstable (Almubarak et al., 2019a,b; Almuntasheri and Operations, 2014). With the need for fracturing in deeper and higher temperature reservoirs, the development of fracturing fluids with superior stability than guar gels is particularly urgent (Hanafy et al., 2021; Phelps et al., 2012).

Synthetic polyacrylamide-based gels are currently the primary choice for fracturing fluids above 180 °C due to their superior thermal stability and cleanliness compared to guar gels (Kamiyama et al., 2022; Wang et al., 2017). Polyacrylamides are mainly composed of two monomers: acrylamide (AM) and acrylic acid (AA). The thermal stability of polyacrylamides could be further improved by introducing acrylamido-2-methylpropanesulfonic acid (AMPS), *N*-vinyl-2-pyrrolidone (NVP), etc. APMS mainly improves the steric resistance of the side chain of the polymer, while NVP improves the rigidity of the main chain of the polymer (Salunkhe et al., 2021). Holtsclaw et al. (2017) developed an AMPS copolymer and the maximum operating temperature of the copolymer gel fracturing fluid reached 204 °C. The upper-temperature limit of the fracturing fluid has been greatly increased, but the shear degradation, high friction, high cost, and reservoir damage of the crosslinked fracturing fluid in the wellbore still limit its application in the ultra-deep reservoirs (Zhang Y. et al., 2018). Delayed crosslinking has been used to extend the crosslinking time of fracturing fluid, enabling them to crosslink in the wellbore or reservoir, effectively reducing shear time and friction (Sokhanvarian et al., 2019; Yang et al., 2020). However, this requires that the fracturing fluid should possess sufficient viscosity and viscoelasticity to maintain proppant suspension properties before crosslinking (Li et al., 2019). The above purpose is typically achieved by increasing the concentration or molecular weight of the polymer, which significantly raises costs. Additionally, gel breaking will be more difficult and reservoir damage is inevitable (Da et al., 2022; Wang J. et al., 2020). Currently, it appears difficult for ultra-deep fracturing fluids to simultaneously meet the requirements of high-temperature resistance, shear resistance, low friction, low cost, and low damage (Manz and Carter, 2017; Wang D. et al., 2020). Therefore, based on the use of the synthetic polyacrylamide-based gel and delayed crosslinking method, it is worth developing a novel polymer system for fracturing fluid that possesses high viscosity and viscoelasticity at low dosages and molecular weight (Liang et al., 2017; Tong and Mohanty, 2016).

Strengthening the intermolecular force is a feasible way to improve the viscosity and viscoelasticity of polymers without increasing the molecular weight and concentration (de Greef and Meijer, 2008; Yu et al., 2021). The electrostatic and hydrophobic properties were introduced into the polymer to synthesize a fracturing fluid that could be applied in high-salt reservoirs reported by Zhang et al. (2022). The fracturing fluid formed by the combination of hydrophobic association polymer and viscoelastic surfactant has high viscoelasticity and shear resistance, as researched by Pu et al. (2018). In this paper, supramolecular forces were introduced to construct a supramolecular polymer system (Almubarak et al., 2019a,b; Ji et al., 2015; Le et al., 2017). Due to the supramolecular interaction between polymer chains, the network structure constructed by supramolecular forces could be formed. Consequently, the supramolecular polymer system possesses a high viscosity and viscoelasticity with a lower concentration and molecular weight, which is used to efficiently suspend the proppant before crosslinking (Panchagnula et al., 2004; Qin et al., 2010). As the temperature increased, the supramolecular polymer system was crosslinked with Zr–crosslinker to form a double network gel, which could compensate for the viscosity loss of the fracturing fluid at high temperatures. In addition, due to the low molecular weight and concentration of the polymer system, a clean fluid would be

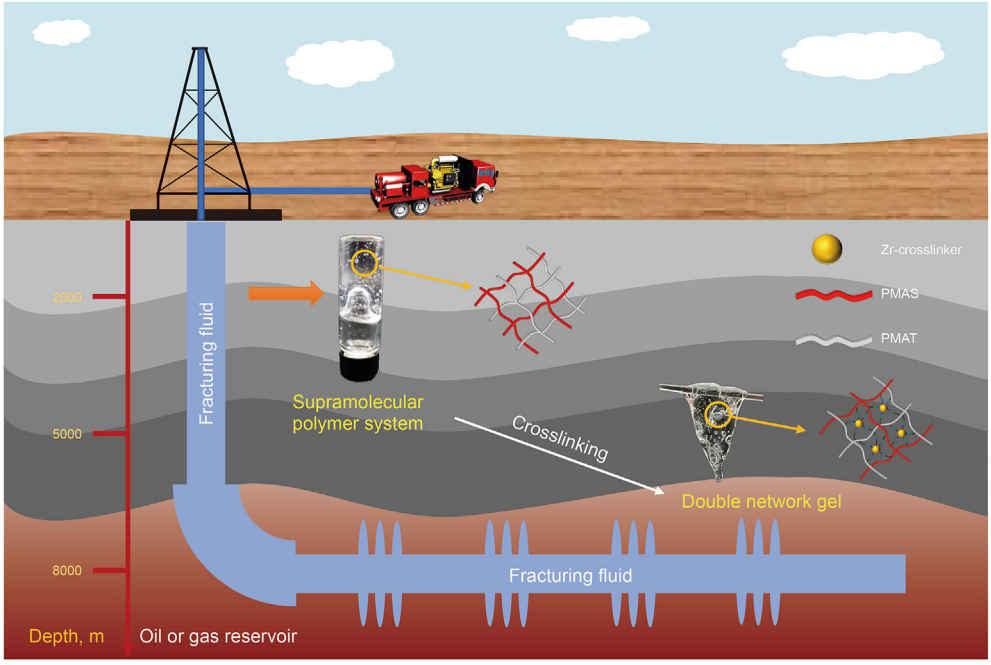

Fig. 1. Diagram of fluids used at different stages of the hydraulic fracturing process.

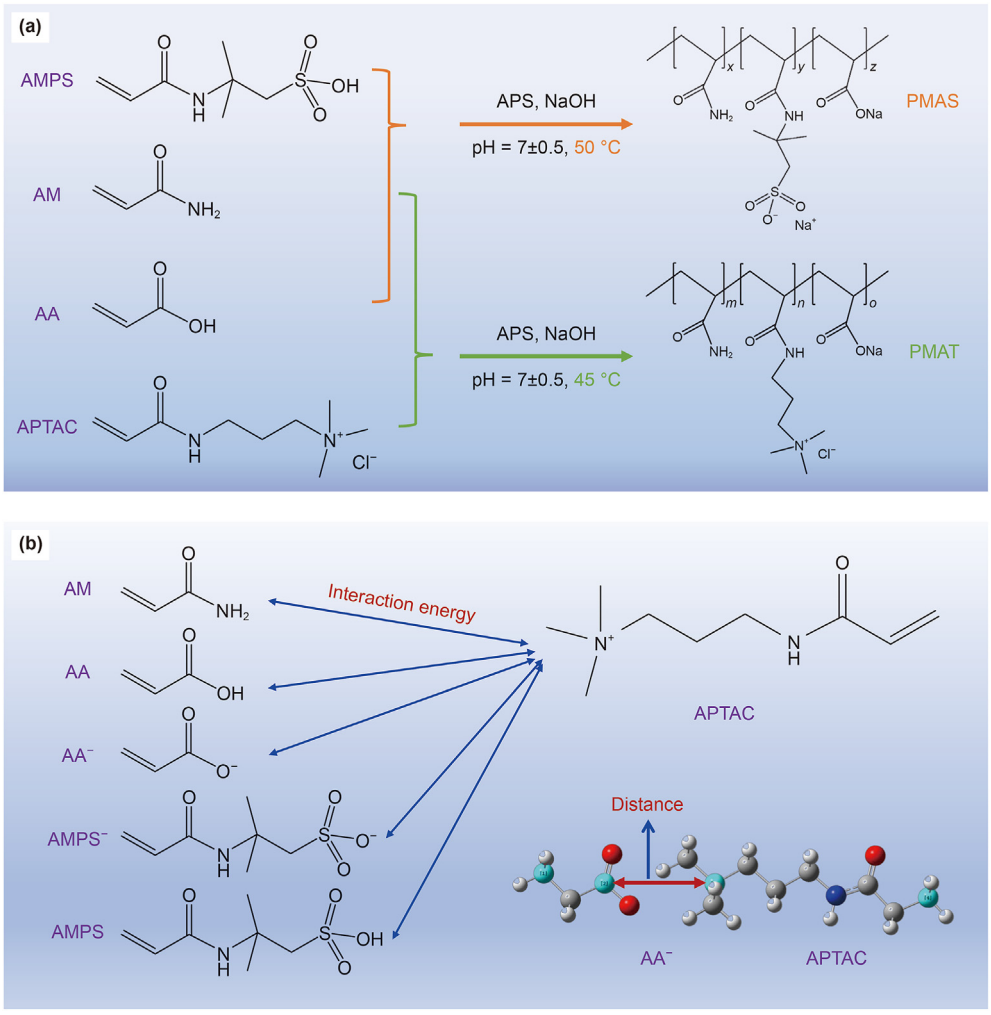

Fig. 2. (**a**) Graphical synthetic routes of PMAS and PMAT; (**b**) Schematic diagram of molecular construction in the quantum chemical calculation (Red balls: oxygen atoms, light blue balls and dark grey balls: carbon atoms, dark blue balls: nitrogen atoms, light grey balls: hydrogen atoms).

obtained after the gel breaking.

A diagram of the ultra-deep reservoir fracturing was shown in Fig. 1, where different fluids were used at different stages to reduce friction and improve the proppant carrying and shear stability. Due to the use of a delayed crosslinker, the fracturing fluid was not immediately crosslinked to reduce friction at the stage of surface and shallow wellbore. Proppant was mainly carried by a supramolecular polymer system with high viscosity and viscoelasticity (Davoodi et al., 2023). As the fracturing fluid reached deeper into the wellbore or reservoir, the double network gel was formed to maintain the shear stability at high temperatures. At the same time, the supramolecular polymer system could also be crosslinked to form a gel at low concentration, which contributes to the cleanliness of the gel-breaking fluid.

2. Materials and methods

2.1. Materials

Acrylamide (AM) (> 99%), acrylic acid (AA) (> 99%), 2-acrylamido-2-methylpropane sulfonic acid (AMPS) (> 99%), poly(-diallyldimethylammonium chloride) (PDDA) (molecular weight of (10–20) × 10^4 g/mol, 20 wt% in water), 3-mercaptopropionic acid (> 98%) and sodium 2-mercaptoethanesulfonate (> 95%) were all purchased from Shanghai Aladdin Biochemical Technology Co. Ltd., Shanghai, China. The Zr-crosslinker is provided by chemical company. The traditional polymer utilized in our paper is a partially hydrolyzed polyacrylamide polymer, primarily comprised of two monomers: AM and AA. The molecular weight of traditional polymer is 1078 × 10^4 g/mol. The traditional polymer is supplied by Dongying Xingjia New Materials Co. Ltd., serving as a thickening agent for the preparation of gel fracturing fluid. (3-acrylamidopropyl) trimethylammonium chloride (APTAC) (74–76 wt% in water) and poly(2-acrylamido-2-methyl-1-propanesulfonic acid) (PAMPS) (molecular weight of 200 × 10^4 g/mol, 15 wt% in water) were purchased from Shanghai Maclin Biochemical Technology Co. Ltd., Shanghai, China. Ammonium persulfate (APS) (> 98%), sodium hydroxide (> 96%), and ethanol (> 99.7%) were purchased from Sinopharm Group Chemical Reagent Co. Ltd., Shanghai, China. Deionized water was provided in our laboratory.

2.2. Methods

2.2.1. Synthesis and characterization of polymers

The synthesis process of polymers (PMAS and PMAT) is shown in Fig. 2(a). A certain amount of AM, AA, AMPS, and deionized water was added to a beaker and stirred until completely dissolved. The

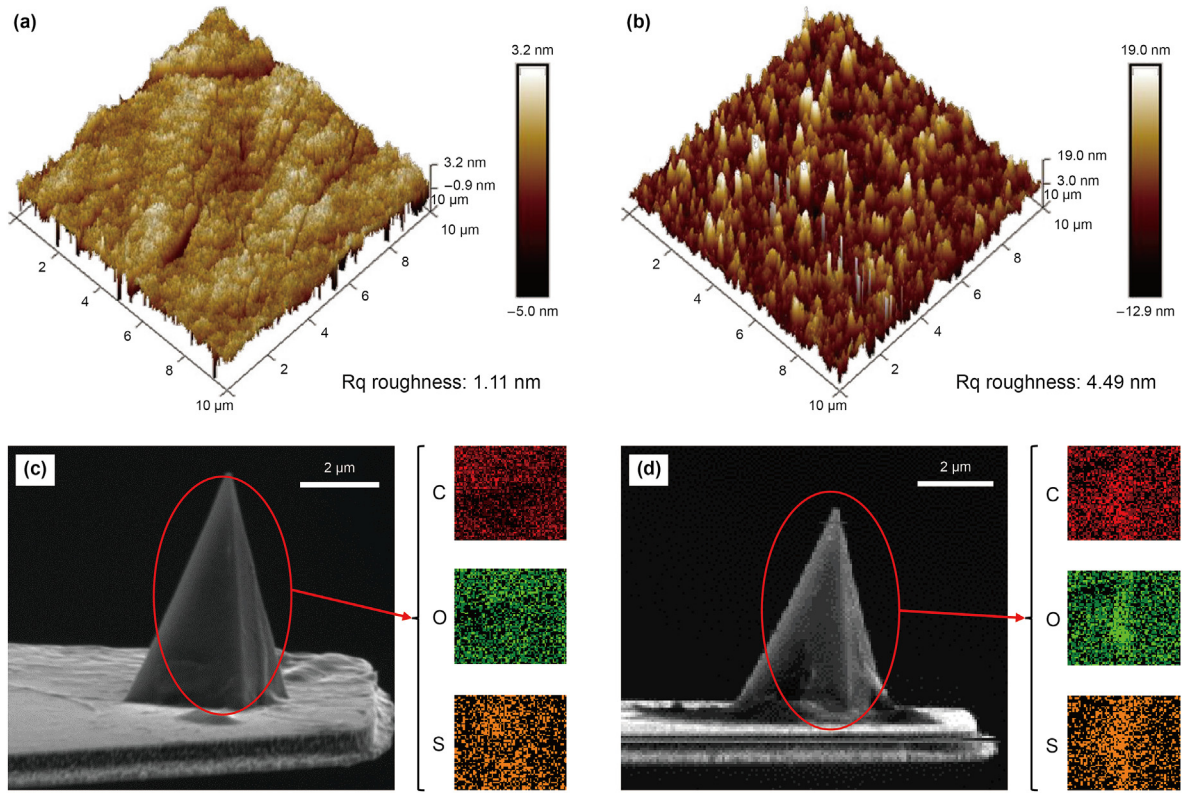

Fig. 3. The basal layer and tip. (**a**) Roughness of the quartz glass sheet; (**b**) Roughness of basal layer with treatment through LBL method; (**c**) The tip modified by sodium 2-mercaptoethanesulfonate; (**d**) The tip modified by sodium mercaptopropionate.

molar ratio of AM:AA:AMPS was controlled at 8:1:1 and NaOH was used to neutralize the pH of the solution to 7±0.5. APS was then added as an initiator, followed by a bubble degassing with nitrogen for 30 min. Finally, the solution was transferred to an oil bath at 50 °C for 6 h until the reaction was completed and the colorless or light white gel was obtained. The gel was dehydrated and washed in ethanol at least 5 times and dried to obtain PMAS after crushing. AMPS was replaced by APTAC and the temperature was reduced to 45 °C to obtain PMAT with other conditions remaining the same. The molecular weights of PMAS (268×10^4 g/mol) and PMAT (380×10^4 g/mol) were measured using a viscosimeter.

Infrared (IR) spectrum and hydrogen nuclear magnetic resonance (^{1}H NMR) spectrum are important representational methods of the chemical structure. In this paper, IR spectra and ^{1}H NMR spectra of the two synthetic polymers were tested respectively to characterize their molecular structures. The IR spectrum was conducted by Thermo Scientific Nicolet IS50 Fourier transform infrared spectrometer (America) and potassium bromide was used for tablet preparation. ^{1}H NMR spectrum was performed using Bruker AV400MHz NMR spectrometer (Switzerland) after the synthetic polymer was dissolved in deuteroxide (D_2O).

2.2.2. Measurement of molecular weight of polymers

The Ubbelohde viscometer was used to measure the average molecular weight of the polymers. A polymer solution with an initial concentration (c_0) of 0.001 g/mL was prepared and diluted to five polymer solutions with a concentration was c_r times the original concentration ($c_r = 1, 2/3, 1/2, 1/3$ and $1/4$). t was the time that five polymer solutions of different concentrations flow through the viscometer. t_0 was the time for the 1.0 mol/L of NaCl solution to flow through the viscometer. The relative viscosity (η_r) and increased viscosity (η_{sp}) of polymers with different concentrations could be calculated according to Eq. (1).

$$\eta_{sp} = (t - t_0) / t_0 = \eta_r - 1 \quad (1)$$

Draw two lines: η_{sp}/c_r–c_r and $\ln\eta_r/c_r$–c_r. H is the intercept value of the intersection point of the two lines at the ordinate. The intrinsic viscosity ($[\eta]$) and molecular weight (M) of the polymers could be calculated according to Eqs. (2) and (3).

$$[\eta] = H / c_0 \quad (2)$$

$$M = 802\,[\eta]^{1.25} \quad (3)$$

2.2.3. Preparation of supramolecular polymer system and double network gel

The supramolecular polymer system consists of PMAS and PMAT, which were first completely dissolved in deionized water and then mixed in a specific proportion. PMAS is the main polymer, and its viscosity and viscoelasticity were regulated by adding PMAT. The double network gel was obtained by dropping a certain amount of Zr-crosslinker into the supramolecular polymer system. The crosslinking time of the double network gel is 3 min. Based on not reducing the elastic modulus G' of the double network gel, the crosslinking time can be further extended to 15 min using sodium lactate solution, as shown in Fig. S1 (Supplementary Material). Hence, the crosslinking time of double network gel in this paper was adjustable in 3–15 min at 25 °C, which meets the requirement time of delayed crosslinking. The crosslinking time of the double network gel was the time when it could be hung with a glass rod after adding a crosslinking agent, as shown in Fig. 1.

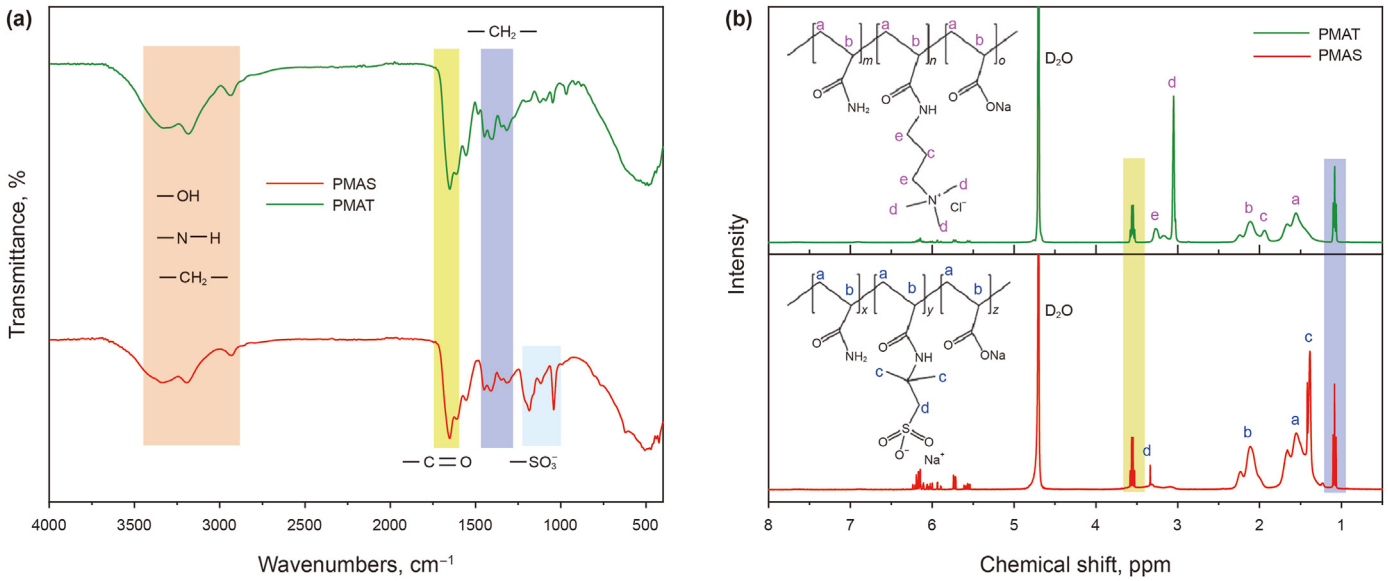

Fig. 4. Structural characterization of synthetic polymers. (**a**) IR spectra; (**b**) ^{1}H NMR spectra.

2.2.4. Rheological test

Rheological performance was measured by the HAKKE RS600B rheometer (Thermo Hakke Corporation, America). In the test of high-temperature shear measurement, the temperature ranged from 25 to 200 °C, the shear rate was fixed at 170 s^{-1}, and a pressure of 2.5 MPa was loaded in advance to prevent the evaporation of the double network gel at high temperatures. The other experiments were carried out at 25±0.5 °C. The shear viscosity was obtained at a shear rate of 170 s^{-1} and the viscoelasticity of polymers was obtained by frequency sweeping with shear stress maintained at 1 Pa. The shear rate range of the variable shear experiment was from 10^{-2}–10^{3} s^{-1}.

2.2.5. Microstructure

Due to its strong electrostatic effect, the supramolecular polymer system might form structures that differ from those of traditional polyacrylamide-based polymers. In this paper, the microstructures of the polymers were measured by a scanning electron microscope (SEM, model JSM-7610F, magnification of 25–10^{6} times) produced by Nippon Electronics.

2.2.6. Quantum chemical calculation

The quantitative chemical calculation method was applied to study the interaction energy between APTAC and other molecules to explore the intrinsic mechanism of the supramolecular polymer system (Fig. 2(b)). In this section, the molecular structure was constructed with Guassview, and four positioned atoms (light blue balls) were kept in a straight line. The distance between two molecules was defined as the distance between the two light blue atoms in the middle. Fixing the APTAC, another molecule was moved horizontally to alter the distance between the two molecules. The energy between the two molecules was calculated after the molecular structure was optimized at each distance.

2.2.7. AFM mechanical test

An atomic force microscope (AFM) (Bruker MultiMode8, Germany) was used for mechanical measurement in our research. A schematic diagram of the mechanical test by AFM was shown in Fig. S2 (Supplementary Material). In this section, 3-mercaptopropionic acid and sodium 2-mercaptoethanesulfonate were respectively modified on gold-plated silicon carbide tips (NPG-10, Brucker) to represent R—COO^{-} and R—SO_3^{-} in synthetic polymers. Studies have shown that a stable Au—S covalent bond could form between the —SH and Au on the surface of the tip (Gao et al., 2018; Ma et al., 2015). The energy dispersive spectroscopy (EDS) analysis of the tip modified with sodium 2-mercaptoethanesulfonate was shown in Fig. 3(c). It could be seen that the modified tip contained a large amount of C, O, and S. The tip modified by sodium mercaptopropionate is displayed in Fig. 3(d). Similarly, the tip contained a large amount of C, O, and S (Zhao et al., 2022). Therefore, it could be concluded that sodium 2-mercaptoethanesulfonate and sodium mercaptopropionate had been attached to the tips respectively from the analysis of EDS.

The root mean square (Rq) roughness of the quartz glass sheet before treatment was 1.11 nm as shown in Fig. 3(a). Quartz glass was used as a substrate, and the basal layer containing R—$N^{+}(CH_3)_3$ was obtained by the layer-by-layer self-assembly method as reported by Yu and Ivanisevic (2004). Pre-washed quartz glass was soaked in 5 g/L PDDA for 20 min and then was washed with deionized water to remove surface retention. Similarly, the washed quartz glass was further soaked in 6.4 g/L PAMPS for 20 min and then was washed with deionized water to remove surface retention. The above operation was repeated to obtain a basal layer of a certain thickness and maintained the outermost surface of the basal layer as PDDA, which was used to represent the R—$N^{+}(CH_3)_3$ in the synthetic polymer. The Rq roughness reached 4.49 nm as exhibited in Fig. 3(b) after treatment by the layer-by-layer (LBL) method.

2.2.8. Proppant suspension and gel-breaking experiment

The sedimentation height of single or multi-particle proppant at different times was recorded to determine the suspension performance of the supramolecular polymer systems. The ceramsite (0.7 ± 0.05 mm diameter) with better shape uniformity was used to replace quartz sand as proppant, and the bulk volume ratio of proppant to polymer solution was 3:10 for the multi-particle proppant suspension experiment.

To obtain a gel-breaking solution, different doses of a gel-breaking agent (APS) were added to the pre-prepared gel. The mixture was placed in a glass tube and heated in an oven at 200 °C

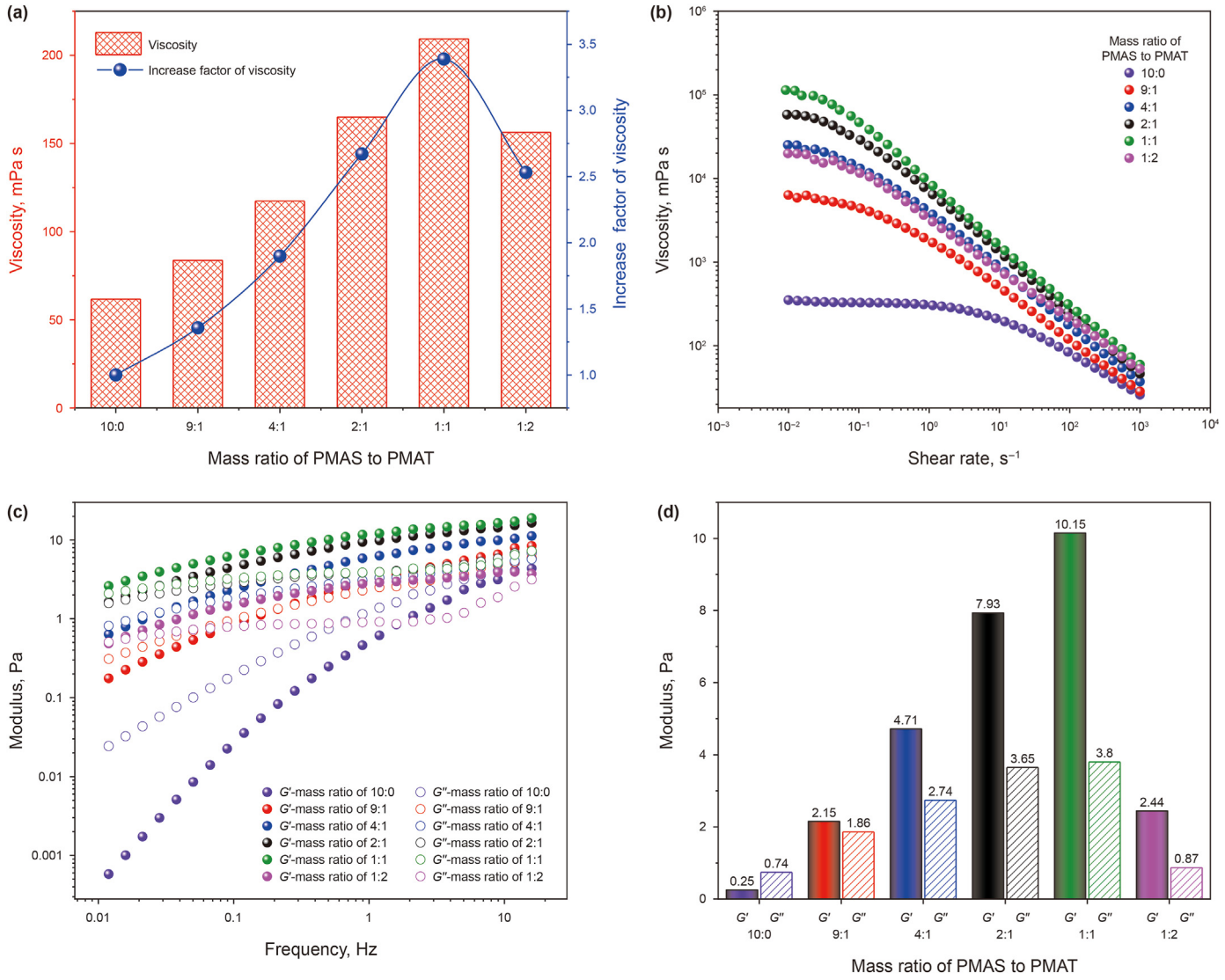

Fig. 5. Viscosity and viscoelasticity of supramolecular polymer system for different mass ratios of PMAS to PMAT when the total mass concentration was 0.4 wt%. (**a**) Shear viscosity and viscosity increase factor at 170 s^{-1}; (**b**) Viscosity vs. shear rate ranging from 10^{-2}–10^{3} s^{-1}; (**c**) Viscoelasticity vs. frequency; (**d**) Viscoelasticity at 0.5 Hz.

for 1 h. Then, the gel-breaking solution was centrifuged at 3000 r/min for two times and dried to obtain residues.

3. Results and discussion

3.1. Structural analysis of polymers

The structures of the polymers were characterized by IR and ^{1}H NMR. As shown in Fig. 4(a), PMAS had an absorption peak of −OH at 3339.59 cm^{-1}, a stretching vibration peak of N−H at 3194.02 cm^{-1}, a stretching vibration peak of $-CH_2-$ at 2931.38 cm^{-1}, and a stretching vibration peak of −C═O at 1651.75 cm^{-1}. The same absorption peak also appeared in PMAT. In addition, the characteristic absorption peaks of $-SO_3$ in AMPS appeared at 1041.23 and 1184.94 cm^{-1}. The ^{1}H NMR of PMAS and PMAT were shown in Fig. 4(b). As seen in Fig. 4(b), the chemical shift (δ) of $-CH_2-$ (a) and −CH− (b) on the main chain of the PMAS occurred at 1.54 and 2.11 ppm, respectively. $\delta = 1.39$ ppm and $\delta = 3.38$ ppm were the peaks of $-CH_3$ (c) and $-CH_2-$ (d) on the side chain of PMAS. As for PMAT, the absorption peaks of $-CH_2-$ (a) and −CH− (b) on the main chain of the PMAT still appeared at 1.56 and 2.11 ppm. $\delta =$ 1.94 ppm, $\delta = 3.27$ ppm, and $\delta = 3.05$ ppm were the peaks of $-CH_2-$ (c, e) and $-CH_3$ (d) on the side chain of PMAT, respectively. The expected molecular structures of polymers were obtained as known from the analysis of IR spectra and ^{1}H NMR spectra.

3.2. Rheological properties and microstructure of supramolecular polymer system

The total concentration was the other important factor affecting the viscosity and viscoelasticity of the supramolecular polymer system. It could be seen from Fig. S3 (Supplementary Material) that the higher the concentration, the higher the viscosity and viscoelastic modulus, and the growth factor of viscosity reached the highest at a concentration of 0.4 wt%. Therefore, the supramolecular polymer system with a concentration of 0.4 wt% was used as the research object in subsequent experiments.

Viscosity and viscoelasticity are important parameters for evaluating the proppant suspension property of fracturing fluid. All rheological tests in this section were conducted at 25 °C. As could be seen from Fig. 5(a), as the PMAT content increased, both the viscosity and the viscosity increase factor of the supramolecular

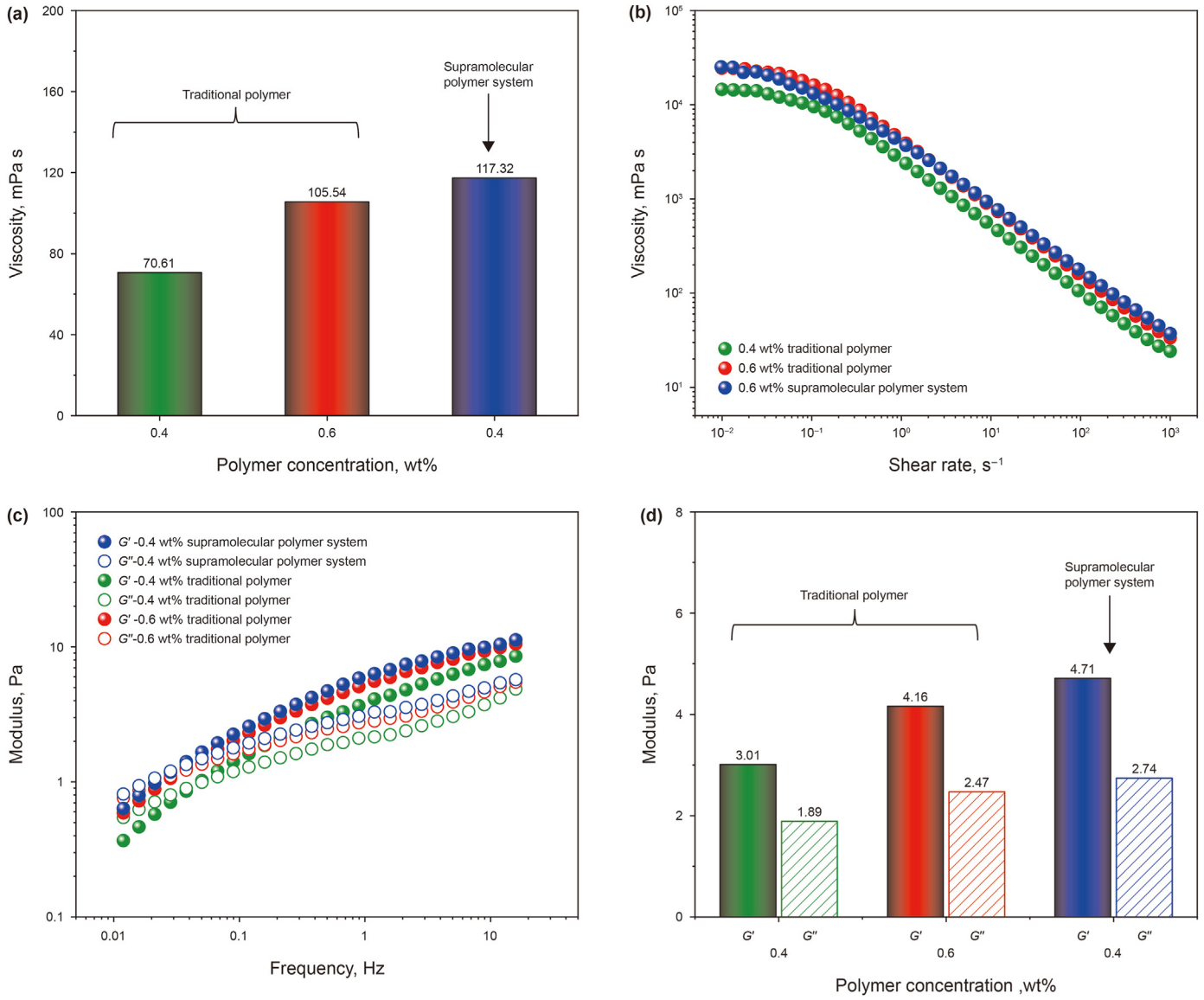

Fig. 6. Viscosity and viscoelasticity of the supramolecular polymer system (the mass ratio of PMAS to PMAT is 4:1) and the traditional polymer. (**a**) Shear viscosity at 170 s^{-1}; (**b**) Viscosity vs. shear rate ranging from 10^{-2}–10^{3} s^{-1}; (**c**) Viscoelasticity vs. frequency; (**d**) Viscoelasticity at 0.5 Hz.

polymer system first increased and then decreased. Both the viscosity (209.34 mPa s) and the viscosity increase factor (3.39 times) reached the maximum value when the mass ratio was 1:1. Due to the presence of cationic monomer APTAC in PMAT, the $R-N^{+}(CH_3)_3$ with positive charge in APTAC would generate strong electrostatic attraction with the $R-SO_3^{-}$ or $R-COO^{-}$ of PMAS, which might be an important factor in the formation of supramolecular polymer system (Deng et al., 2020; Schulze and Kirstein, 2005). Therefore, as the increase in PMAT concentration, the content of $R-N^{+}(CH_3)_3$ in the polymer solution gradually increased, leading to an increase in viscosity. However, the content of $R-N^{+}(CH_3)_3$ should be controlled within a certain range. When the content of $R-N^{+}(CH_3)_4$ was too high, the electrostatic attraction in the polymer solution would be strengthened, causing flocculation and weakening the viscosity of the polymer. A small amount of white precipitation in the solution was observed at a mass ratio of 1:2 (Fig. 5(d)). As exhibited in Fig. 5(b), the viscosity difference of the supramolecular polymer system was mainly reflected in the low shear rate range with viscosity ranging from 351 to 113842 mPa s at 0.01 s^{-1}, reaching the maximum when the mass ratio was 1:1. Different from the viscosity at 170 s^{-1}, the viscosity of the supramolecular polymer system with a mass ratio of 1:2 was lower than that of 4:1 at 0.01 s^{-1}, possibly because the production of white precipitates reduces the network structural strength of the supramolecular polymer system. The same conclusion could also be drawn from the viscoelastic experiment in Fig. 5(c), which showed that both the elastic modulus (G') and viscosity modulus (G'') of the supramolecular polymer system with the mass ratio of 1:2 was less than that of 4:1. The G' was greater than the G'' across all frequency ranges for the mass ratios of 2:1, 1:1, and 1:2. However, in the low-frequency region, the G'' was higher than the G' for the mass ratios of 9:1 and 4:1. On the contrary, the G'' was higher than the G' for the mass ratio of 10:0 in all frequency ranges. The electrostatic attraction was weak due to the low $R-N^{+}(CH_3)_3$ content in the case of 9:1 and 4:1. It could also be seen from Fig. 5(d) that the G' of the supramolecular polymer system had reached 7.93 and 10.15 Pa, respectively, at the mass ratio of 2:1 and 1:1, while the G' of the supramolecular polymer system at the mass ratio of 4:1 was only 4.71 Pa. However, the G' of

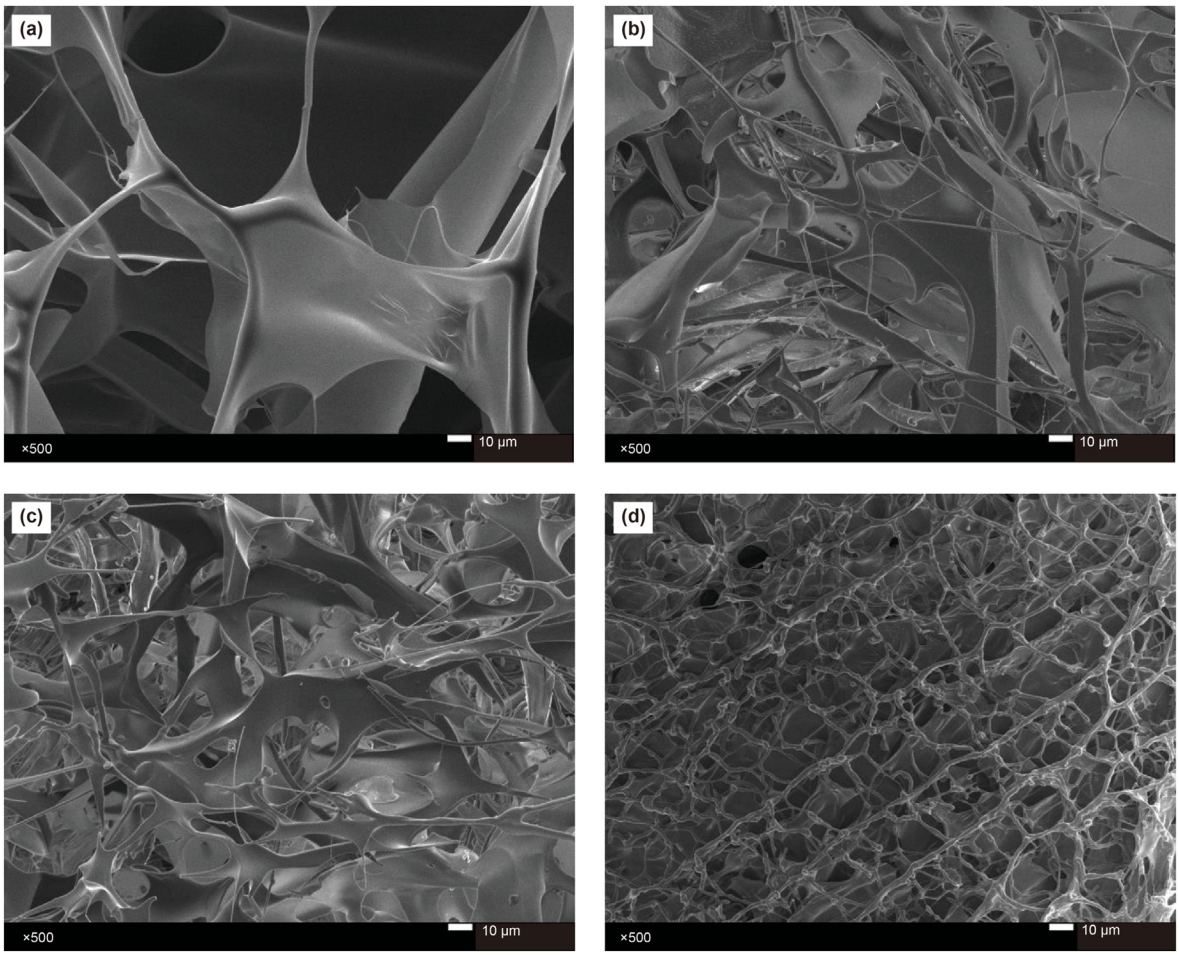

Fig. 7. SEM images of (**a**) 0.4 wt% PMAS, (**b**) 0.4 wt% traditional polymer, (**c**) 0.6 wt% traditional polymer, and (**d**) supramolecular polymer system with the mass ratio of PMAS to PMAT of 4:1.

the supramolecular polymer system was much higher than the G'' at the mass ratio of 4:1, and the viscosity at 170 s^{-1} had reached 117.32 mPa s, which had exceeded the minimum standard for the viscosity (> 50 mPa s) of the fracturing fluid before crosslinking. The price of PMAT is higher than that of PMAS. Based on meeting the viscosity and viscoelasticity improvement, PMAT should not be too high due to its high cost. As a result, the mass ratio of 4:1 was a more reasonable choice.

Based on the above experiments, the supramolecular polymer system could maintain high viscosity and viscoelasticity through supramolecular interaction under the low molecular weight (268×10^4 g/mol). The comparison of rheological properties of the supramolecular polymer system and the traditional polymer (hydrolyzed polyacrylamide with a molecular weight of 1078×10^4 g/mol) was shown in Fig. 6. Both the viscosity and viscoelasticity of the 0.4 wt% supramolecular polymer system were much higher than those of the traditional polymer at the same concentration and were slightly higher than those of the 0.6 wt% traditional polymers. Therefore, without increasing the molecular weight, the supramolecular system with a concentration of 0.4 wt% achieved the viscosity and viscoelasticity comparable to the 0.6 wt% traditional polymers.

The SEM images of PMAS, traditional polymer, and the supramolecular polymer system were shown in Fig. 7. The microstructure of the supramolecular polymer system exhibited characteristics similar to that of a gel, showing high viscoelasticity (Minami et al., 2019; Roullet et al., 2020). The microstructures of PMAS and the traditional polymer were similar to traditional polymers with lamellar structure and irregularity (Zhao et al., 2019). The microstructure of the supramolecular polymer system was ordered, similar to the layer-by-layer (LBL) structure that differed from PMAS and the traditional polymer. This difference might be due to the stacking of layers between PMAS and PMAT, which generates an ordered spatial network structure through supramolecular interaction (Wang et al., 2014; Wu et al., 2019).

3.3. Intrinsic interaction mechanism of supramolecular polymer system

In this section, quantum chemical calculations and AFM techniques were employed to gain deeper insights into the interaction mechanism of the supramolecular polymer system. As could be seen from Fig. 8(a), the electrostatic attraction was observed between APTAC and other molecules. The electrostatic energy between AA^-/$AMPS^-$ and APTAC was much greater than that of the other three monomers. The result was obvious because APTAC is positively charged, while AA^- and $AMPS^-$ are negatively charged. Similarly, the exchange energy between AA^-/$AMPS^-$ and APTAC was higher than other molecules (Fig. S4 in Supplementary Material). As observed in Fig. 8(b), the variation trends of induction energy were similar to electrostatic energy, and the absolute value was slightly lower than that of electrostatic energy. The

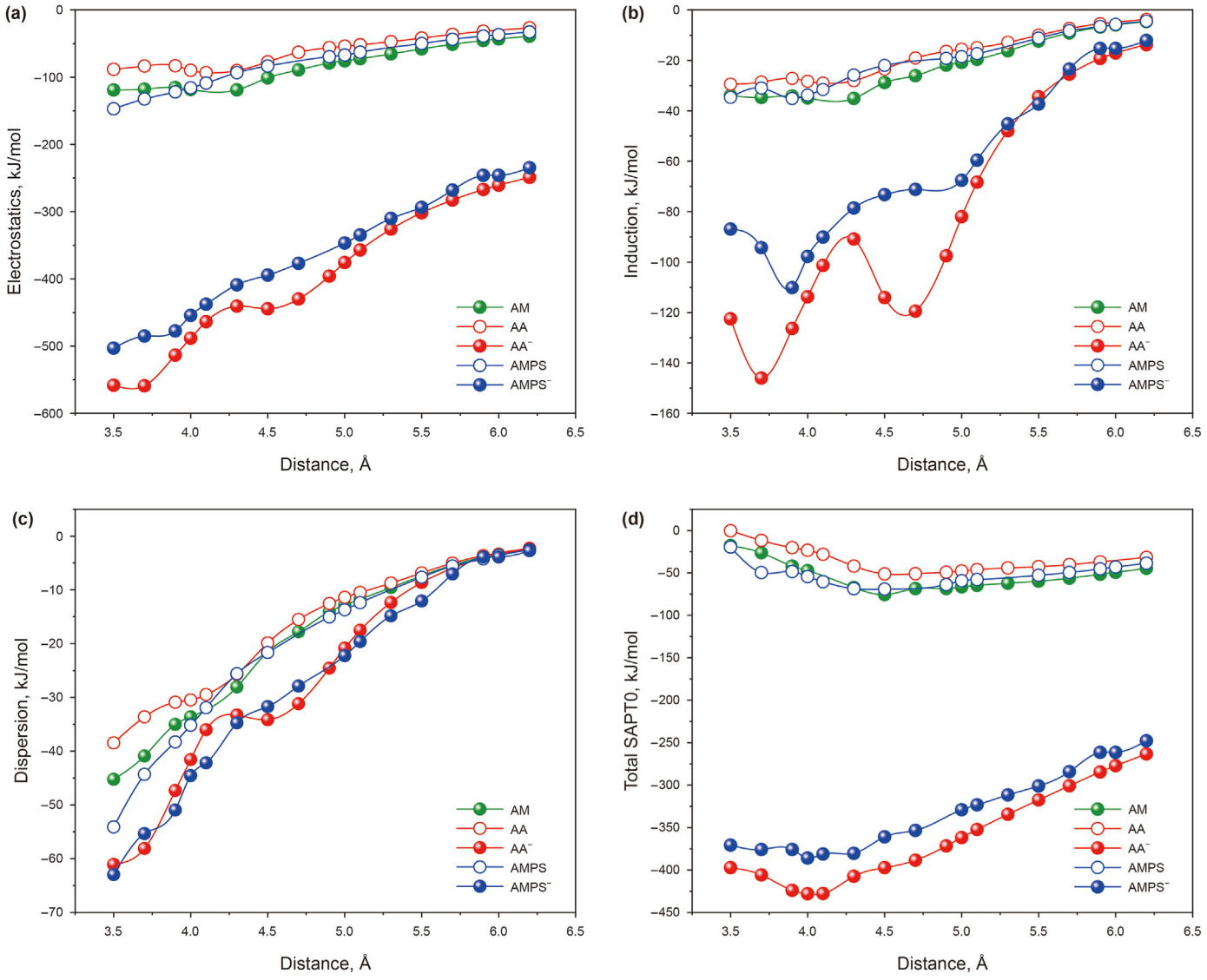

Fig. 8. Interaction energy between APTAC and other monomers with quantum chemical calculation. (**a**) Electrostatic energy; (**b**) Induction energy; (**c**) Dispersion energy; (**d**) Total SAPT0.

interaction between AA^-/$AMPS^-$ and APTAC on induction energy was also stronger than other molecules. The variation trends of induction energy and dispersion energy were similar, but the difference was not large for all molecules (Fig. 8(c)). Total SAPT0 was the sum of electrostatic energy, exchange energy, induction energy, and dispersion energy as displayed in Fig. 8(d). The equilibrium distance of AA^- and $AMPS^-$ was at 4.0 Å, and the total SAPT0 of AA^- and $AMPS^-$ reached −428.00 and −385.83 kJ/mol, respectively. From the results of quantitative chemical calculation, the electrostatic interaction was an important factor affecting the intermolecular force, and the effect of AA^- was slightly stronger than that of $AMPS^-$. However, $R-COO^-$ and $R-SO_3^-$ were fully ionized in quantitative chemical calculations, which might differ from their true force with $R-N^+(CH_3)_3$ in water environments for $R-COO^-$ was easily hydrolyzed in water. Therefore, AFM would be used to further investigate the force between the $R-N^+(CH_3)_3$ and the $R-COO^-$/$R-SO_3^-$ in water environments.

The tips and the substrate have been modified by predefined molecules, respectively, from the characterization results in Section 2.2.7. The typical force curves are shown in Fig. 9(a). When retracting the tip, the adhesion force was recorded. 256 force curves were obtained by measuring in 500 nm × 500 nm region. Then, the adhesion force of each force curve was calculated through frequency distribution, as shown in Fig. 9(b) and (c). The median adhesion force was 0.526 and 0.414 nN for $R-COO^-$ and $R-SO_3^-$, respectively. To further reduce the experimental error, mechanical measurements were conducted in three different regions to obtain average adhesion force, as shown in Fig. 9(d).

The average adhesion forces were 0.530 nN between $R-COO^-$ and $R-SO_3^-$ and 0.377 nN between $R-COO^-$ and $R-N^+(CH_3)_3$, respectively. The conclusion was that the interaction between $R-COO^-$ and $R-N^+(CH_3)_3$ was slightly stronger than that of $R-SO_3^-$, which was also consistent with the results of quantum chemistry calculation. Therefore, the main conclusion was that the interaction mechanism of the supramolecular polymer system was the interaction between PMAS and PMAT, in which the electrostatic interaction dominated. The electrostatic interaction mainly came from the electrostatic attraction between $R-COO^-$/$R-SO_3^-$ in PMAS and

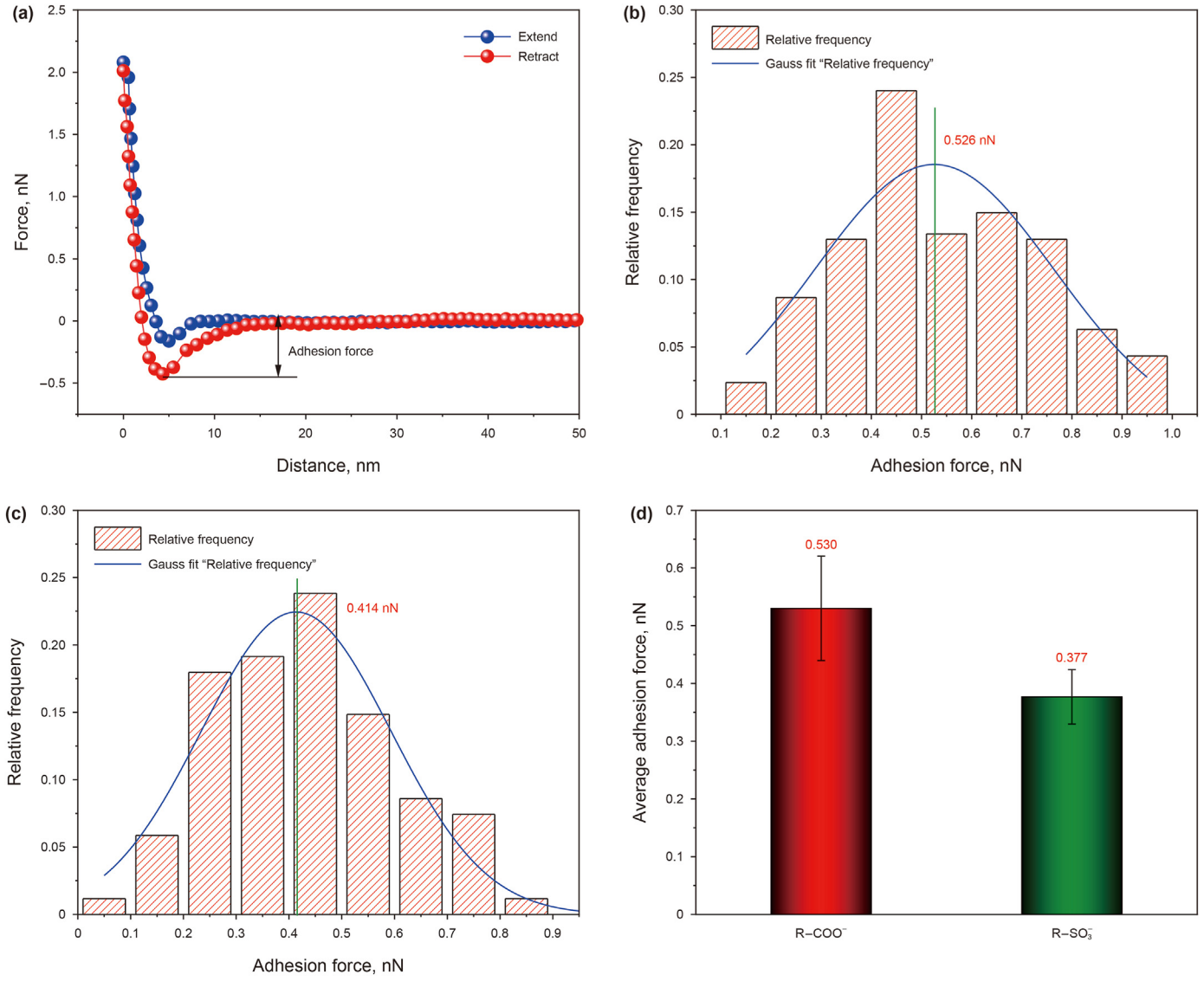

Fig. 9. Diagram of the force between R–$N^+(CH_3)_3$ and R–COO^-/R–SO_3^-. (**a**) Typical force curve between R–COO^-/R–SO_3^- and R–$N^+(CH_3)_3$; (**b**) Frequency distribution of adhesion force between R–COO^- and R–$N^+(CH_3)_3$; (**c**) Frequency distribution of adhesion force between R–SO_3^- and R–$N^+(CH_3)_4$; (**d**) Average adhesion force.

R–$N^+(CH_3)_3$ in PMAT.

3.4. Viscoelasticity of double network gel

As the fracturing fluid was injected into the reservoir, the supramolecular polymer system gradually crosslinked to form gels. High-strength gels are crucial for the fracturing fluid to effectively transport proppants at high temperatures (Sun et al., 2015). Therefore, it was necessary to investigate the viscoelasticity of double network gel. In this section, the viscoelasticity between different polymers and Zr-crosslinker was investigated, as shown in Fig. 10. For a supramolecular polymer system, the double network gel with hanging ability could be formed when the Zr-crosslinker concentration was 0.05–0.4 wt%, as exhibited in Fig. 10(a) and (d). When the Zr-crosslinker concentration was 0.3 wt%, G' reached its maximum and then decreased, which might be due to over-crosslinking caused by the excessive crosslinking agent. Surprisingly, the supramolecular polymer system could form a high-strength gel only at the crosslinker concentration of 0.05 wt%, which was conducive to reducing the cost of fracturing fluids. By comparison, it can be found that a hangable gel could be obtained only when the concentration of the Zr-crosslinker was greater than 0.6 wt% at 0.4 wt% traditional polymer (Fig. 10(b) and (e)) and all of G' was less than 5 Pa for all crosslinker concentration, which was much less than 0.4 wt% supramolecular polymer system. When the concentration of traditional polymer reached 0.6 wt% (Fig. 10(c) and (f)), effective crosslinking could occur only when the concentration of Zr-crosslinker was greater than 0.2 wt%, and the G' was still lower than 0.4 wt% supramolecular polymer system. Therefore, it could be concluded that the supramolecular polymer system could form double network gel at lower dosages of polymer and crosslinker, reducing the costs and potentially reducing residue after gel breaking (Huang et al., 2020; Lu et al., 2017).

Shear viscosity was also an essential property of gel fracturing fluids, especially the shear dilution and shear recovery. As revealed in Fig. S5 (Supplementary Material), both double network gels and traditional gels exhibit shear-thinning characteristics. However, the viscosity of double network gels surpasses that of traditional gels at the shear rate of 170 s^{-1}. Furthermore, the shear recovery rate of the double network gel stands at 73.3%, which is significantly higher

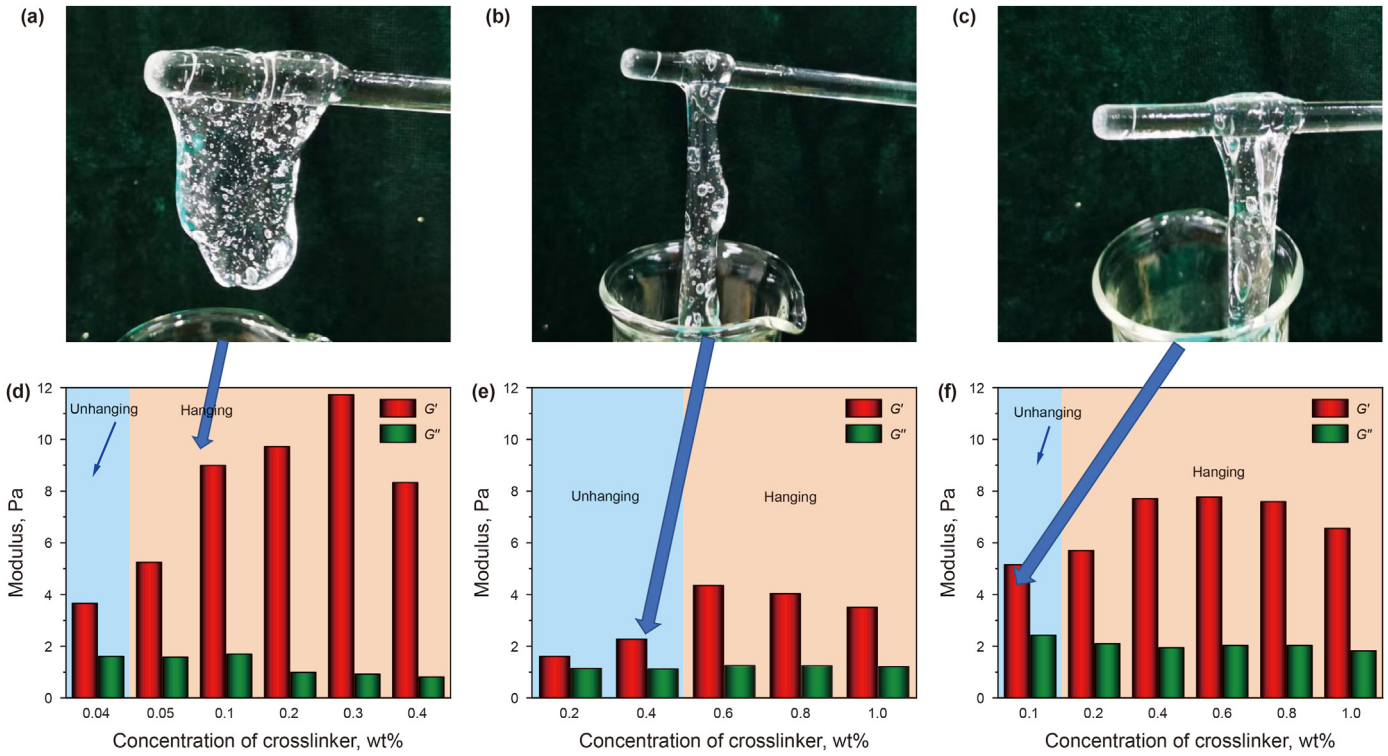

Fig. 10. Photographs and viscoelasticity of gels formed by Zr-crosslinker and different polymers. (**a**) and (**d**) 0.4 wt% supramolecular polymer system; (**b**) and (**e**) 0.4 wt% traditional polymer; (**c**) and (**f**) 0.6 wt% traditional polymer.

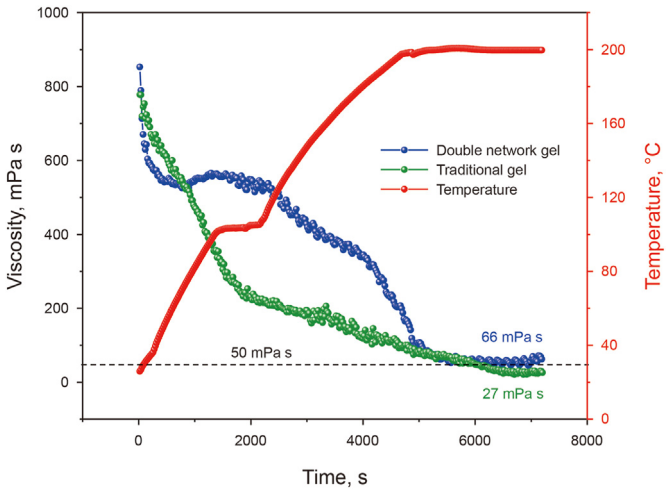

Fig. 11. High-temperature shear measurement. Double network gel: 0.4 wt% supramolecular polymer system + 0.1 wt% Zr-crosslinker. Traditional gel: 0.6 wt% traditional polymer + 0.6 wt% Zr-crosslinker.

than the 53.5% recovery rate of the traditional gel, indicating superior shear resistance.

3.5. Application performance of fracturing fluid

It had been proved that the supramolecular polymer system possessed good viscosity and viscoelasticity, which could form double network gel at low dosage. In the following, the shear stability at high temperatures, the gel breaking of double network gel, and the proppant suspension property of the supramolecular polymer system will be demonstrated.

Temperature and shear resistance are crucial factors in determining the applicability of double network gel in ultra-deep/ultra-high temperature fracturing to evaluate these properties, a high-temperature shear test was conducted on the double network gel, and the results are presented in Fig. 11. The viscosity of the double network gel decreased rapidly at first and then stabilized between 530 and 560 mPa s at 100 °C. As the temperature continued to rise, the viscosity continued to decline. When the temperature reached 200 °C, the viscosity decreased to 168 mPa s. After shearing for 2 h, the average viscosity at the last minute was taken as the final stable

Table 1
Experimental results of gel breaking.

Sample No.	Polymer	Zr-crosslinker concentration, wt%	G' of gel, Pa	APS concentration, wt%	Residue content, mg/L
#1	0.4 wt% supramolecular polymer system	0.1	8.84	0.01	50
#2				0.05	0
#3				0.10	0
#4	0.6 wt% traditional polymer	0.6	7.77	0.01	340
#5				0.05	160
#6				0.10	20

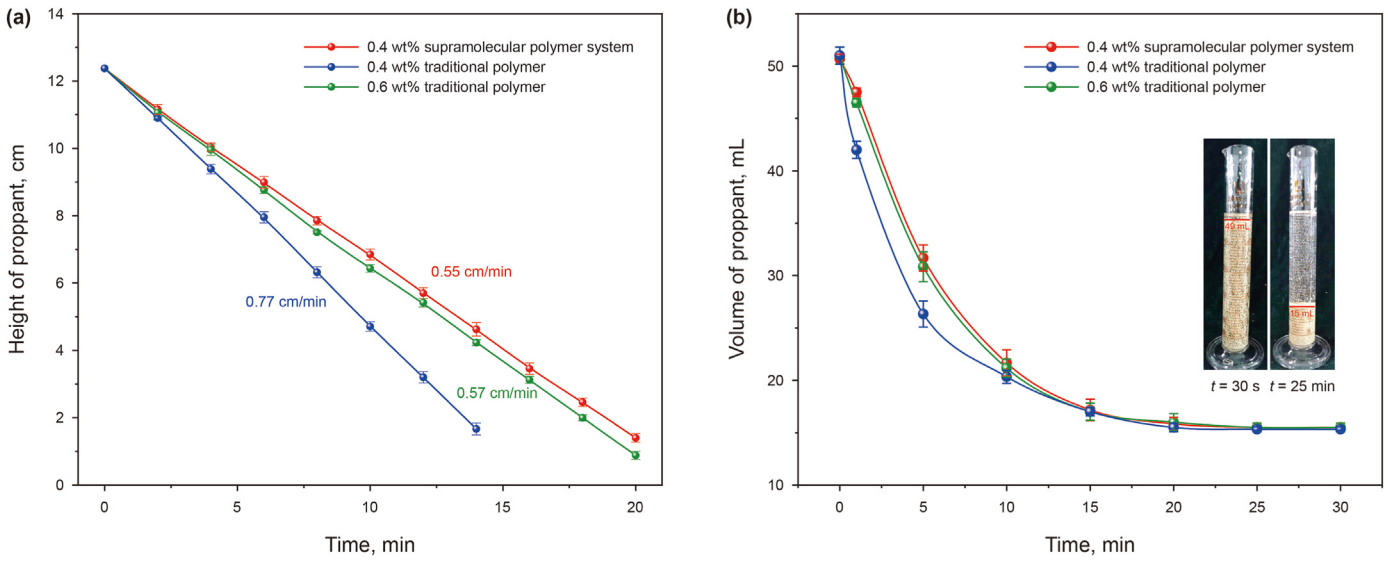

Fig. 12. Sedimentation of particles in different polymer solutions. (**a**) Single particle proppant; (**b**) Multi-particle proppant.

value, which was 66 mPa s, meeting the viscosity standard (> 50 mPa s) of high-temperature shear measurement of fracturing fluid (Yang et al., 2020). Therefore, the double network gel met the temperature resistance requirement of the fracturing fluid at 200 °C. In contrast, the viscosity of the traditional gel decreased rapidly at the beginning and continued to decline until the final viscosity was 27 mPa s, which was significantly lower than the specified viscosity. The network structure of the traditional gel was solely based on a Zr crosslinked network, making it difficult to recover after shearing, compared with the network formed by the supramolecular force.

The results of the gel breaking are shown in Table 1. Two groups of gels with similar elastic modulus were compared. The gel-breaking solutions of #4 and #5 were relatively muddy, and obvious sediment could be observed at the bottom of the tube after centrifugation (Fig. S6 in Supplementary Material). It could be seen from Table 1 that when the concentration of APS reached 0.05 wt%, the double network gel was completely broken without residues. This was due to the low concentrations of polymer and crosslinker used in the double network gel system. In contrast, the traditional gel could not be completely broken at the low concentration of APS, resulting in residue contents of 340 mg/L at 0.01 wt% APS and 160 mg/L at 0.05 wt% APS. Excessive residue content could lead to reservoir damage and reduce the seepage capability of oil and gas reservoirs after fracturing (Zhou et al., 2020). When the APS concentration was 0.1 wt%, the residue content was reduced to 0. Although at high APS content, the gel fracturing fluid could be broken completely without residue content. However, it was clear that excessive APS could cause the gel to degrade too quickly, which affected the transport of the proppant (Das et al., 2018; Wang J. et al., 2020). In conclusion, the supramolecular polymer system could form a double network gel with a low concentration of polymer and crosslinker, which contributed to the gel breaking at a low concentration of APS.

The settlement of a single proppant particle in a polymer solution was described in Fig. 12(a). The proppant settlement rate was the fastest in the 0.4 wt% traditional polymer solution, reaching 0.77 cm/min. The sedimentation rate of the proppant was equal by comparing the 0.4 wt% supramolecular polymer system with the 0.6 wt% traditional polymer. The sedimentation test of multi-particle proppant was described in Fig. 12(b). The suspension performance of the polymer was 0.4 wt% supramolecular polymer system > 0.6 wt% traditional polymer > 0.4 wt% traditional polymer, which was consistent with the conclusion obtained from the single proppant particle sedimentation experiment. The difference in the multi-particle sedimentation experiment was that the sedimentation of the upper part proppant was influenced by the presence of the bottom proppant, resulting in a decrease in the volume decline rate over time. This could be due to the interaction among particles, which led to a more gradual settling behavior.

4. Conclusions

In this study, a supramolecular polymer system tailored for ultra-deep fracturing fluid was developed, of which viscosity and viscoelasticity were investigated and the interaction mechanism was revealed. The application performance of the fracturing fluid was demonstrated in the end. The key findings of this study were summarized below.

(1) The viscosity and viscoelasticity of the supramolecular polymer system could be regulated by changing the concentration and mass ratio of PMAS to PMAT. The 0.4 wt% supramolecular polymer system (molecular weight of (268–380) × 10^4 g/mol) could achieve similar viscosity and viscoelasticity to that of the 0.6 wt% traditional polymer (molecular weight of 1078 × 10^4 g/mol).

(2) The supramolecular polymer system had an ordered network structure similar to gels. The formation of this structure was mainly caused by the electrostatic attraction between R–SO_3^-/R–COO^- in PMAS and R–$N^+(CH_3)_3$ in PMAT, of which the role of R–COO^- (0.526 nN) was slightly greater than that of R–SO_3^- (0.414 nN).

(3) The supramolecular polymer system could form double network gel with high elastic modulus (9.00 Pa) under only 0.1 wt% Zr-crosslinker, compared to 7.77 Pa of the traditional gel at 0.6 wt% Zr-crosslinker.

(4) The viscosity of the double network gel met the required viscosity (50 mPa s) of the fracturing fluid at 200 °C and could be broken completely under 0.05 wt% APS, which greatly reduced the reservoir damage. The high viscosity and viscoelasticity greatly improved the proppant suspension

property of the supramolecular polymer system at lower molecular weight and concentration.

CRediT authorship contribution statement

Yong-Ping Huang: Writing – original draft, Methodology, Data curation, Conceptualization. **Yong Hu:** Methodology, Investigation, Data curation. **Chang-Long Liu:** Software, Investigation, Data curation. **Yi-Ning Wu:** Writing – review & editing, Supervision, Methodology, Funding acquisition. **Chen-Wei Zou:** Visualization, Software, Data curation. **Li-Yuan Zhang:** Writing – review & editing, Validation, Project administration, Methodology. **Ming-Wei Zhao:** Validation, Supervision, Project administration. **Cai-Li Dai:** Resources, Funding acquisition, Formal analysis, Conceptualization.

Declaration of competing interest

The authors declare that they have no known competing financial interests or personal relationships that could have appeared to influence the work reported in this paper.

Acknowledgments

This study is financially supported by the National Natural Science Foundation of China (Nos. 52120105007 and 52374062) and the Innovation Fund Project for Graduate Students of China University of Petroleum (East China) supported by "the Fundamental Research Funds for the Central Universities" (23CX04047A).

Appendix A. Supplementary data

Supplementary data to this article can be found online at https://doi.org/10.1016/j.petsci.2024.03.018.

References

Alarawi, A., Busaleh, A., Saleh, T.A., et al., 2023. High thermal stability of foams stabilized by graphene oxide and zwitterionic surfactant nanocomposites for fracturing applications. Fuel 332, 126156. https://doi.org/10.1016/j.fuel.2022.126156.

Almubarak, T., Alkhaldi, M., Ng, J.H., et al., 2019a. Design and application of high-temperature raw-seawater-based fracturing fluids. SPE J. 24 (4), 1929–1946. https://doi.org/10.2118/195597-PA.

Almubarak, T., Ng, J.H., Nasr-El-Din, H.A., et al., 2019b. Dual-polymer hydraulic-fracturing fluids: a synergy between polysaccharides and polyacrylamides. SPE J. 24 (6), 2635–2652. https://doi.org/10.2118/191580-PA.

Almuntasheri, G., Operations, 2014. A critical review of hydraulic-fracturing fluids for moderate- to ultralow-permeability formations over the last decade. SPE Prod. Oper. 29 (4), 243–260. https://doi.org/10.15530/urtec-2023-3871053.

Biheri, G., Imqam, A., 2022. Proppant transport using high-viscosity friction reducer fracture fluids at high-temperature environment. SPE J. 27 (1), 60–76. https://doi.org/10.2118/206750-PA.

Da, Q., Yao, C., Zhang, X., et al., 2022. Investigation on microscopic invasion characteristics and retention mechanism of fracturing fluid in fractured porous media. Petrol. Sci. 19 (4), 1745–1756. https://doi.org/10.1016/j.petsci.2022.03.009.

Das, A., Chauhan, G., Verma, A., et al., 2018. Rheological and breaking studies of a novel single-phase surfactant-polymeric gel system for hydraulic fracturing application. J. Petrol. Sci. Eng. 167, 559–567. https://doi.org/10.1016/j.petrol.2018.04.033.

Davoodi, S., Al-Shargabi, M., Wood, D., et al., 2023. A comprehensive review of beneficial applications of viscoelastic surfactants in wellbore hydraulic fracturing fluids. Fuel 338, 127228. https://doi.org/10.1016/j.fuel.2022.127228.

de Greef, T., Meijer, E., 2008. Materials science - supramolecular polymers. Nature 453 (7192), 171–173. https://doi.org/10.1038/453171a.

Deng, Z., He, Y., Wang, Y., et al., 2020. Chondroitin sulfate hydrogels based on electrostatic interactions with enhanced adhesive properties: exploring the bulk and interfacial contributions. Soft Matter 16 (26), 6128–6137. https://doi.org/10.1039/d0sm00547a.

Gao, M., Zhang, M., Du, H., et al., 2023. A novel triple responsive smart fluid for tight oil fracturing-oil expulsion integration. Petrol. Sci. 20 (2), 982–992. https://doi.org/10.1016/j.petsci.2023.01.008.

Gao, Z., Xie, L., Cui, X., et al., 2018. Probing anisotropic surface properties and surface forces of fluorite crystals. Langmuir 34 (7), 2511–2521. https://doi.org/10.1021/acs.langmuir.7b04165.

Hanafy, A., Najem, F., Nasr-El-Din, H., 2021. Effect of nanoparticle shape on viscoelastic surfactant performance at high temperatures. SPE J. 26 (3), 1436–1454. https://doi.org/10.2118/203836-PA.

Holtsclaw, J., Galindo, G., Chopade, P., 2017. Next-generation boron-crosslinked fracturing fluids: breaking the lower limits on polymer loadings. SPE Prod. Oper. 32 (4), 440–448. https://doi.org/10.2118/174988-PA.

Hu, R., Zhao, J., Wang, Y., et al., 2019. A highly stretchable, self-healing, recyclable and interfacial adhesion gel: preparation, characterization and applications. Chem. Eng. J. 360, 334–341. https://doi.org/10.1016/j.cej.2018.12.001.

Huang, Q., Liu, S., Wang, G., et al., 2019. Coalbed methane reservoir stimulation using guar-based fracturing fluid: a review. J. Nat. Gas Sci. Eng. 66, 107–125. https://doi.org/10.1016/j.jngse.2019.03.027.

Huang, Q., Liu, S., Cheng, W., et al., 2020. Fracture permeability damage and recovery behaviors with fracturing fluid treatment of coal: an experimental study. Fuel 282, 118809. https://doi.org/10.1016/j.fuel.2020.118809.

Ji, X., Shi, B., Wang, H., et al., 2015. Supramolecular construction of multifluorescent gels: interfacial assembly of discrete fluorescent gels through multiple hydrogen bonding. Adv. Mater. 27 (48), 8062–8066. https://doi.org/10.1002/adma.201504355.

Kamiyama, Y., Tamate, R., Hiroi, T., et al., 2022. Highly stretchable and self-healable polymer gels from physical entanglements of ultrahigh-molecular weight polymers. Sci. Adv. 8 (42). https://doi.org/10.1126/sciadv.add0226.

Le, X., Rioux, L., Turgeon, S., 2017. Formation and functional properties of protein-polysaccharide electrostatic hydrogels in comparison to protein or polysaccharide hydrogels. Adv. Colloid Interface Sci. 239, 127–135. https://doi.org/10.1016/j.cis.2016.04.006.

Li, X., Yin, H., Zhang, R., et al., 2019. A salt-induced viscosifying smart polymer for fracturing inter-salt shale oil reservoirs. Petrol. Sci. 16 (4), 816–829. https://doi.org/10.1007/s12182-019-0329-3.

Liang, F., Al-Muntasheri, G., Ow, H., et al., 2017. Reduced-polymer-loading, high-temperature fracturing fluids by use of nanocrosslinkers. SPE J. 22 (2), 622–631. https://doi.org/10.2118/177469-pa.

Lu, Y., Yang, F., Ge, Z., et al., 2017. Influence of viscoelastic surfactant fracturing fluid on permeability of coal seams. Fuel 194, 1–6. https://doi.org/10.1016/j.fuel.2016.12.078.

Luo, J., Cao, H., Chiarella, D., et al., 2023. Ultra-deep carbonate basement reservoirs formed by polyphase fracture-related karstification in the Offshore Bohai Bay Basin, China. Petrol. Sci. 20 (4), 2009–2025. https://doi.org/10.1016/j.petsci.2023.03.021.

Ma, C., Wang, C., Acevedo-Velez, C., et al., 2015. Modulation of hydrophobic interactions by proximally immobilized ions. Nature 517 (7534), 347–U443. https://doi.org/10.1038/nature14018.

Manz, K., Carter, K., 2017. Investigating the effects of heat activated persulfate on the degradation of furfural, a component of hydraulic fracturing fluid chemical additives. Chem. Eng. J. 327, 1021–1032. https://doi.org/10.1016/j.cej.2017.06.168.

Minami, S., Suzuki, D., Urayama, K., 2019. Rheological aspects of colloidal gels in thermoresponsive microgel suspensions: formation, structure, and linear and nonlinear viscoelasticity. Curr. Opin. Colloid Interface Sci. 43, 113–124. https://doi.org/10.1016/j.cocis.2019.04.004.

Panchagnula, V., Jeon, J., Dobrynin, A., 2004. Molecular dynamics simulations of electrostatic layer-by-layer self-assembly. Phys. Rev. Lett. 93 (3), 037801. https://doi.org/10.1103/PhysRevLett.93.037801.

Phelps, E., Enemchukwu, N., Fiore, V., et al., 2012. Maleimide cross-linked bioactive peg hydrogel exhibits improved reaction kinetics and cross-linking for cell encapsulation and in situ delivery. Adv. Mater. 24 (1), 64–70. https://doi.org/10.1002/adma.201103574.

Pu, W., Du, D., Liu, R., 2018. Preparation and evaluation of supramolecular fracturing fluid of hydrophobically associative polymer and viscoelastic surfactant. J. Petrol. Sci. Eng. 167, 568–576. https://doi.org/10.1016/j.petrol.2018.04.032.

Qin, Y., Wang, Y., Tang, M., et al., 2010. Layer-by-layer electrostatic self-assembly of anionic and cationic carbon nanotubes. Chin. Chem. Lett. 21 (7), 876–879. https://doi.org/10.1016/j.cclet.2010.02.003.

Roullet, M., Clegg, P., Frith, W., 2020. Rheology of protein-stabilised emulsion gels envisioned as composite networks 1-Comparison of pure droplet gels and protein gels. J. Colloid Interface Sci. 579, 878–887. https://doi.org/10.1016/j.jcis.2020.05.004.

Salunkhe, B., Schuman, T., Al, Brahim, A., et al., 2021. Ultra-high temperature resistant preformed particle gels for enhanced oil recovery. Chem. Eng. J. 426, 130712. https://doi.org/10.1016/j.cej.2021.130712.

Schulze, K., Kirstein, S., 2005. Layer-by-layer deposition of TiO_2 nanoparticles. Appl. Surf. Sci. 246 (4), 415–419. https://doi.org/10.1016/j.apsusc.2004.11.064.

Shu, Y., Yan, J., 2008. Characterization and prevention of formation damage for fractured carbonate reservoir formations with low permeability. Petrol. Sci. 5 (4), 326–333. https://doi.org/10.1007/s12182-008-0055-8.

Sokhanvarian, K., Nasr-El-Din, H., Harper, T., 2019. Effect of ligand type attached to zirconium-based crosslinkers and the effect of a new dual crosslinker on the properties of crosslinked carboxymethylhydroxypropylguar. SPE J. 24 (4), 1741–1756. https://doi.org/10.2118/194204-pa.

Somoza, A., Garcia-Mayoral, M., Soto, A., 2023. A formulation based on a cationic surface-active ionic liquid and an anionic surfactant for enhanced oil recovery at a carbonate reservoir. Fuel 346, 128363. https://doi.org/10.1016/

j.fuel.2023.128363.
Sun, Z., Lv, F., Cao, L., et al., 2015. Multistimuli-responsive, moldable supramolecular hydrogels cross-linked by ultrafast complexation of metal ions and biopolymers. Angew. Chem. Int. Ed. 54 (27), 7944–7948. https://doi.org/10.1002/anie.201502228.
Tong, S., Mohanty, K., 2016. Proppant transport study in fractures with intersections. Fuel 181, 463–477. https://doi.org/10.1016/j.fuel.2016.04.144.
Wang, D., Sun, Y., Tsang, D., et al., 2020. The roles of suspended solids in persulfate/Fe^{2+} treatment of hydraulic fracturing wastewater: synergistic interplay of inherent wastewater components. Chem. Eng. J. 388, 124243. https://doi.org/10.1016/j.cej.2020.124243.
Wang, J., Huang, Y., Zhang, Y., et al., 2020. Study of fracturing fluid on gel breaking performance and damage to fracture conductivity. J. Petrol. Sci. Eng. 193, 107443. https://doi.org/10.1016/j.petrol.2020.107443.
Wang, L., Long, Y., Ding, H., et al., 2017. Mechanically robust re-crosslinkable polymeric hydrogels for water management of void space conduits containing reservoirs. Chem. Eng. J. 317, 952–960. https://doi.org/10.1016/j.cej.2017.02.140.
Wang, R., Bi, S., Guo, Z., et al., 2022. Molecular insight into replacement dynamics of CO_2 enhanced oil recovery in nanopores. Chem. Eng. J. 440, 135796. https://doi.org/10.1016/j.cej.2022.135796.
Wang, S., Zhang, Y., Guo, J., et al., 2014. A study of relation between suspension behavior and microstructure and viscoelastic property of guar gum fracturing fluid. J. Petrol. Sci. Eng. 124, 432–435. https://doi.org/10.1016/j.petrol.2014.09.016.
Wang, X., Zhao, M., Wang, X., et al., 2023. Synergistic effect of dual hydrogen-donor deep eutectic solvent for performance improvement of fracturing-oil expulsion fluids. Chem. Eng. J. 468, 143728. https://doi.org/10.1016/j.cej.2023.143728.
Wu, A., Gao, Y., Zheng, L., 2019. Zwitterionic amphiphiles: their aggregation behavior and applications. Green Chem. 21 (16), 4290–4312. https://doi.org/10.1039/c9gc01808e.
Wu, Y., Tang, L., Li, Y., et al., 2023. Probing the influence of secondary fracture connectivity on fracturing fluid flowback efficiency. Petrol. Sci. 20 (2), 973–981. https://doi.org/10.1016/j.petsci.2022.10.014.
Xu, H., Li, Y., Yu, G., et al., 2023. The enhancement of performance and imbibition effect of slickwater-based fracturing fluid by using MoS_2 nanosheets. Petrol. Sci. 20 (4), 2187–2201. https://doi.org/10.1016/j.petsci.2022.12.008.
Xu, K., Yang, H., Zhang, H., et al., 2022. Fracture effectiveness evaluation in ultra-deep reservoirs based on geomechanical method, Kuqa Depression, Tarim Basin, NW China. J. Petrol. Sci. Eng. 215, 110604. https://doi.org/10.1016/j.petrol.2022.110604.
Yang, B., Wang, H., Li, G., et al., 2022. Fundamental study and utilization on supercritical CO_2 fracturing developing unconventional resources: current status, challenge and future perspectives. Petrol. Sci. 19 (6), 2757–2780. https://doi.org/10.1016/j.petsci.2022.08.029.
Yang, X., Mao, J., Zhang, W., et al., 2020. Tertiary cross-linked and weighted fracturing fluid enables fracture stimulations in ultra high pressure and temperature reservoir. Fuel 268, 117222. https://doi.org/10.1016/j.fuel.2020.117222.
Yu, J., Wang, K., Fan, C., et al., 2021. An ultrasoft self-fused supramolecular polymer hydrogel for completely preventing postoperative tissue adhesion. Adv. Mater. 33 (16), 2008395. https://doi.org/10.1002/adma.202008395.
Yu, M., Ivanisevic, A., 2004. Encapsulated cells: an atomic force microscopy study. Biomaterials 25 (17), 3655–3662. https://doi.org/10.1016/j.biomaterials.2003.10.061.
Zhang, H., Liu, S., Xiao, H., 2018. Frictional behavior of sliding shale rock-silica contacts under guar gum aqueous solution lubrication in hydraulic fracturing. Tribol. Int. 120, 159–165. https://doi.org/10.1016/j.triboint.2017.12.044.
Zhang, Q., Mao, J., Yang, X., et al., 2022. Synthesis of a hydrophobic association polymer with an inner salt structurefor fracture fluid with ultra-high-salinity water. Colloids Surf., A 636, 128062. https://doi.org/10.1016/j.colsurfa.2021.128062.
Zhang, Y., Mao, J., Zhao, J., et al., 2018. Preparation of a novel ultra-high temperature low-damage fracturing fluid system using dynamic crosslinking strategy. Chem. Eng. J. 354, 913–921. https://doi.org/10.1016/j.cej.2018.08.021.
Zhao, G., Chu, Z., Wang, F., et al., 2022. Probing the interaction mechanism between alkanes and hydrophobic substrate using atomic force microscopy and molecular dynamics simulation. SPE J. 27 (3), 1436–1446. https://doi.org/10.2118/209230-pa.
Zhao, T., Zhang, Y., Peng, G., et al., 2019. A branched hydrophobicity associated with polyacrylamide based on silica: synthesis and solution properties. J. Polym. Res. 26 (11). https://doi.org/10.1007/s10965-019-1883-5.
Zhou, H., Huang, X., Liang, Y., et al., 2020. Enhanced bioremediation of hydraulic fracturing flowback and produced water using an indigenous biosurfactant-producing bacteria *acinetobacter* sp. Y2. Chem. Eng. J. 397, 125348. https://doi.org/10.1016/j.cej.2020.125348.